Dynamic Characteristics of a Cavitating Propeller

In this section we examine the unsteady flow characteristics manifest by a cavitating propeller in a water tunnel. To include the unsteady flow contributions it is necessary to revisit and revise the basic conservation results presented in section (Mfc). One intermediate objective will be to identify the dynamic transfer function for a cavitating propeller in a water tunnel. This is a necessary prerequisite to understanding global instabilities of such flows such as the surge instability observed and documented by Duttweiler and Brennen (2002). Another potential application is to the sometimes severe structural vibration that can arise due to the interaction between the cavitation on a ship propeller and the wake of hull. The large body of work on propeller-hull interactions has been summarized by Weitendorf (1989).
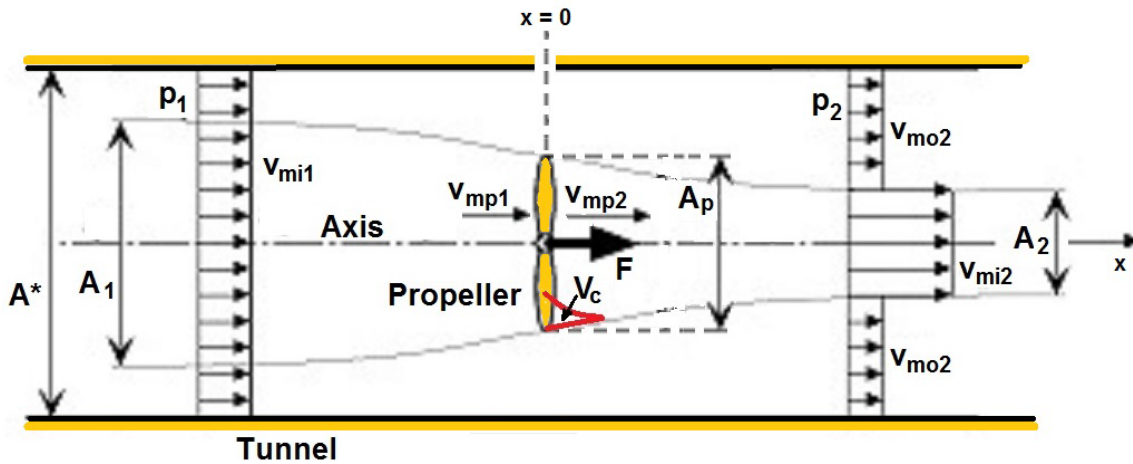

Figure 1: Schematic and notation of a propeller in a tunnel; the cavitation volume is shown in red.

Consider the one-dimensional unsteady, incompressible flow through a propeller (either cavitating or non-cavitating) in a water tunnel as shown in Figure 1. The propeller (cross-sectional area A_p) is located on the centerline of the tunnel whose cross-sectional area is A^*. We consider a stream tube containing the propeller. For simplicity, it will be assumed that the flow is uniformly distributed across the propeller stream tube and is one-dimensional. Friction and mixing losses between the inner and outer flows are neglected.

The analysis parallels that for steady flow detailed in sections (Mfc) and (Mfg) and the notation is the same as that used in those sections. Mass conservation requires that

$$v_{mi1}A_1 - v_{mp1}A_p = -\int_{-\infty}^{0} \frac{\partial A(x,t)}{\partial t}\, dx \tag{Mfh1}$$

$$v_{mi2}A_2 - v_{mp2}A_p = \int_{0}^{\infty} \frac{\partial A(x,t)}{\partial t}\, dx \tag{Mfh2}$$

$$v_{mp2}A_p - v_{mp1}A_p = \frac{dV_c}{dt}\, dt \tag{Mfh3}$$

$$v_{mi2}A_2 + v_{mo2}(A^* - A_2) - v_{mi1}A^* = \frac{dV_c}{dt}\, dt \tag{Mfh4}$$

The right-hand-sides of equations (Mfh1) and (Mfh2) represent the volume change of the stream tube upstream and downstream of the propeller; later these will be ignored for simplicity. The relation between the pressures far upstream and far downstream is obtained by applying Bernoulli's equation in the outer flow as follows:

$$p_2 - p_2 = \frac{1}{2}\rho\left\{v_{mi1}^2 - v_{mo2}^2\right\} - \rho\int_{-\infty}^{\infty}\frac{\partial v_{mo}(x,t)}{\partial t}\,dx \tag{Mfh5}$$

where the last term of the right-hand-side is the inertia effect in the control volume.

Now, we calculate the thrust force F produced by the propeller by applying three basic equations. First, applying the momentum theorem to a control volume containing all the tunnel flow, we obtain;

$$\rho v_{mi1}^2 A^* + p_1 A^* + F = \rho v_{mo2}^2(A^* - A_2) + \rho v_{mi2}^2 A_2 + p_2 A^* + \frac{dM}{dt} \tag{Mfh6}$$

The last term in the right-hand-side is rate of the change of the momentum in the control volume, represented by

$$\begin{aligned}\frac{dM}{dt} &= \rho\frac{d}{dt}\left[\int_{-\infty}^{\infty}\left\{v_{mi}(x,t)A(x,t) + v_{mo}(x,t)(A^* - A(x,t))\right\}dx\right] \\ &= \rho\frac{d}{dt}\left[\int_0^{\infty}\frac{dV_c}{dt}\,dx + A^*\int_{-\infty}^{\infty}v_{mi1}dx\right] = \rho\int_0^{\infty}\frac{d^2V_c}{dt^2}\,dx + \rho A^*\int_{-\infty}^{\infty}\frac{dv_{mi1}}{dt}\,dx\end{aligned} \tag{Mfh7}$$

which yields

$$\begin{aligned}F &= \frac{1}{2}\rho(v_{mi1} - v_{mo2})A^*(2v_{mi2} + v_{mo2} - v_{mi1}) + \rho(v_{mi2} + v_{mo2})\frac{dV_c}{dt} \\ &\quad + \left[\rho A^*\int_{-\infty}^{\infty}\frac{\partial(v_{mi1} - v_{mo}(x,t))}{\partial t}\,dx + \rho\int_0^{\infty}\frac{d^2V_c}{dt^2}\,dx\right]\end{aligned} \tag{Mfh8}$$

Second, we obtain the total pressure difference across the propeller, Δp^T, from the Euler head,

$$\Delta p^T = \rho R\Omega v_{\theta p2} = \rho R\Omega(R\Omega - v_{mp2}\cot\beta) - \rho\frac{c}{\sin\beta}\frac{dv_{mp2}}{dt} \tag{Mfh9}$$

The last term in this equation represents the inertia effect of the fluid in the blade passage. Since the static pressure difference, $p_{p2} - p_{p1}$, is given by

$$p_{p2} - p_{p1} = \frac{1}{2}\rho\left\{R^2\Omega^2 - v_{mp2}^2\cot\beta\right\} - \rho\frac{c}{\sin\beta}\frac{dv_{mp2}}{dt} \tag{Mfh10}$$

the thrust force can be computed as

$$\begin{aligned}F &= (p_{p2} - p_{p1})A_p + \rho\left\{v_{mp2}^2 - v_{mp1}^2\right\}A_p \\ &= \frac{1}{2}\rho\left\{R^2\Omega^2 - v_{mp2}^2\cot\beta\right\}A_p + \rho(v_{mp2} + v_{mp1})\frac{dV_c}{dt} - \rho\frac{A_pc}{\sin\beta}\frac{dv_{mp2}}{dt}\end{aligned} \tag{Mfh11}$$

Third, the pressures p_{p1} and p_{p2} may be related to the upstream and downstream conditions using Bernoulli's equation:

$$p_{p1} = p_1 + \frac{1}{2}\rho v_{mi1}^2 - \frac{1}{2}\rho v_{mp1}^2 - \rho\int_{-\infty}^0\frac{\partial v_{mi}(x,t)}{\partial t}\,dx \tag{Mfh12}$$

where the last term is the inertance in the stream tube. Applying Bernoulli's equation between the outlet of the propeller and far downstream, we obtain

$$p_{p2} = p_2 + \frac{1}{2}\rho\left[v_{mi2}^2 + v_{\theta p2}^2(A_p/A_2)\right] - \frac{1}{2}\rho\left[v_{mp2}^2 + v_{\theta p2}^2\right] + \rho\int_0^{\infty}\frac{\partial v_{mi}(x,t)}{\partial t}\,dx$$

$$= p_2 + \frac{1}{2}\rho v_{mi2}^2 - \frac{1}{2}\rho v_{mp2}^2 + \frac{1}{2}\rho \left[R\Omega - v_{mp2}\cot\beta\right]^2 \left[(A_p/A_2) - 1\right] + \rho \int_0^\infty \frac{\partial v_{mi}(x,t)}{\partial t}\, dx \quad \text{(Mfh13)}$$

Then the thrust force F follows as

$$F = (p_{p2} - p_{p1})A_p + \rho \left\{v_{mp2}^2 - v_{mp1}^2\right\}A_p$$

$$= \frac{1}{2}\rho \left[\left\{v_{mi2}^2 - v_{mo2}^2\right\} + \left\{R\Omega - v_{mp2}\cot\beta\right\}^2 \left\{(A_p/A_2) - 1\right\}\right]A_p$$

$$-\frac{1}{2}\rho(v_{mp2} + v_{mp1})\frac{dV_c}{dt} + \rho A_p \int_0^\infty \frac{\partial(v_{mi}(x,t) - v_{mo}(x,t))}{\partial t}\, dx \quad \text{(Mfh14)}$$

For the purpose of the general discussion, we have considered all possible unsteady effects in the above

formulation, namely the effects of volume change of the stream tubes in equations (Mfh1) and (Mfh2), the inertia effects upstream and downstream of the propeller in equations (Mfh5), (Mfh8) and (Mfh14), and the inertia effect in the propeller in equation (Mfh11) as well as the effects of the cavity volume change dV_c/dt in equations (Mfh3) and (Mfh4). To evaluate many of these terms, we would need to know the shape of the stream tube, which is beyond the scope of the present one-dimensional stream tube analysis. Consequently, some compromises are needed in order to proceed. First we neglect the stream tube volume changes in equations (Mfh1) and (Mfh2) on the basis that these cancel and thus produce no net perturbation within the water tunnel; this may need further examination. Second, we neglect the inertance terms in equations (Mfh5), (Mfh8) and (Mfh14) on the basis that past experience has suggested that we can consider these contributions to be lumped into the other inertance contributions in the tunnel circuit. Again this may need additional examination. In summary, we choose to examine only the unsteady effects associated with dV_c/dt in equations (Mfh3) and (Mfh4).

Summarizing, we note that the eight equations (Mfh1) through (Mfh14) contain eight unknowns v_{mo2}, v_{mi2}, v_{mp2}, v_{mp1}, A_1, A_2, F, and p_2 assuming that the propeller operating parameters v_{mi1}, p_1, $R\Omega$, the discharge flow angle, β, and the rate of change of the cavity volume, dV_c/dt, are given. The empirical relations for the deviation angle that were described in section (Mfg) will be used again here.

To complete the set of governing equations we need to establish a functional expression for the cavity volume, V_c. Consistent with the understanding developed in the context of cavitating pumps it will be assumed that cavity volume, $V_c(p_{p1}, v_{mp1})$, is a function of the inlet pressure p_{p1} and inflow velocity v_{mp1}. Then, the rate of change of the cavity volume can be expressed as

$$\frac{dV_c}{dt} = -K\frac{dp_{p1}}{dt} - M\frac{dv_{mp1}}{dt} \quad \text{(Mfh15)}$$

where $K = -\partial V_c/\partial p_{p1}$ and $M = -\partial V_c/\partial v_{mp1}$ are respectively the cavitation compliance and the mass flow gain factor (Brennen and Acosta 1973). These important parameters are non-dimensionalized as follows;

$$\frac{K^*}{2\pi} = -\frac{\partial(V_c/A_p R)}{\partial \sigma^*} = \frac{\rho R\Omega^2}{2A_p}\frac{\partial V_c}{\partial p_{p1}} = \frac{\rho\Omega^2}{2\pi R}K \quad \text{(Mfh16)}$$

$$M^* = -\frac{\partial(V_c/A_p R)}{\partial(v_{mp1}/R\Omega)} = \frac{\Omega}{A_p}\frac{\partial V_c}{\partial v_{mp1}} = \frac{\Omega}{\pi R^2}M \quad \text{(Mfh17)}$$

where K^* and M^* are the non-dimensional values of the cavitation compliance and the mass flow gain factor used by Duttweiler and Brennen (2002). In this study, the values of K and M are estimated using free streamline theory (Otsuka *et al.* 1996, Watanabe *et al.* 1998).

Given the steady operating characteristics developed in sections (Mfc) and (Mfg), it is valuable to consider the quasi-static response to low frequency fluctuations of the incoming flow velocity, v_{mi1}. For illustrative purposes, we compare the case of $A^*/A_p = 2$ with that for a pump ($A^*/A_p = 1$). Consider first the case when the advance ratio is larger than the critical advance ratio. As the upstream flow velocity varies, the flow rate through the propeller varies less when $A^*/A_p = 2$ than when $A^*/A_p = 1$ (Figure 1 of section (Mfg)). However, when the advance ratio is smaller than the critical value, this trend is reversed. If the propeller were cavitating, these results would suggest that, at larger advance ratios, the mass flow gain factor will be smaller for $A^*/A_p = 2$ than that for $A^*/A_p = 1$, whereas at smaller advance ratios, the mass flow gain factor will be larger for $A^*/A_p = 2$. This is important since the mass flow gain factor is responsible for cavitation instabilities of turbomachinery and a large mass flow gain factor implies a more unstable system.

The surge instability of a cavitating propeller, reported by Duttweiler and Brennen (2002), is an example of cavitation instability caused by a positive mass flow gain factor. They examined two different configurations of the propeller, one in which the propeller is operated in front of a support fairing, and the other in which the propeller is operated downstream of that fairing, and observed a violent surge instability only for the latter case. The explanation for this difference is unknown, but one explanation might be as follows. The presence of the fairing can be considered to be the blockage, so that the effective flow path upstream of the propeller is smaller for the case with the propeller operated downstream of the fairing. Figure 2 of section (Mfc) indicates that the critical value of the advance ratio is larger when the propeller is operated in the narrower duct. So, as the advance ratio decreases, the propeller could readily shift into operation as a pump. The result would be that the mass flow gain factor is larger for the propeller operated downstream of the fairing.

We proceed to analyze the low frequency unsteady characteristics of the cavitating propeller. The system of equations consists of non-linear equations. However, in order to utilize the conventional transfer function methodology, we linearize the problem. For example, the upstream flow velocity is expressed by

$$v_{mi1} = \bar{v}_{mi1} + Re\left\{\tilde{v}_{mi1}e^{j\omega t}\right\} \tag{Mfh18}$$

After substituting similar expressions for all the unknowns, equations (Mfh1)-(Mfh14) are then divided into steady and unsteady parts and linearized under the assumption of small fluctuations. The unsteady parts of the equations consist of linear equations for the unsteady components, the eight unknowns v_{mo2}, v_{mi2}, v_{mp2}, v_{mp1}, A_1, A_2, F, and p_2 as well as the quantities, v_{mi1}, p_1, β and dV_c/dt. The unsteady component of β is obtained by the linearized version of the equation for β in section (Mfg), which diminishes for larger values of σ. The rate of change of cavity volume, dV_c/dt, is given by equation (Mfh15).

Using the equations documented above, we can relate the downstream fluctuations to the inlet fluctuations using the conventional transfer matrix (Brennen 1994):

$$\left\{\begin{array}{c}\tilde{p}_2^T \\ \tilde{m}_2\end{array}\right\} = \begin{bmatrix}T_{11} & T_{12} \\ T_{21} & T_{22}\end{bmatrix}\left\{\begin{array}{c}\tilde{p}_1^T \\ \tilde{m}_1\end{array}\right\} \tag{Mfh19}$$

where p^T and m are total pressure and mass flow rate, respectively.

Figure 2 presents a typical calculation of the transfer matrix for an advance ratio of $J_1 = 1.0$ and duct cross-sectional areas of $A^*/A_p = 1$, 2 and 10. For illustrative purposes, values of the compliance and mass flow gain factor ($K^*/2\pi$, M^*) of $(0.1, 1.0)$ are selected since these values are typical of those obtained by previous researchers (Brennen 1994). The change of the exit flow angle β is neglected for simplicity, assuming $\sigma = \infty$. Note that T_{21} takes a similar value for all cases while there are large differences in the other elements of transfer matrix. If we consider the case with no discharge mass flow fluctuations, the
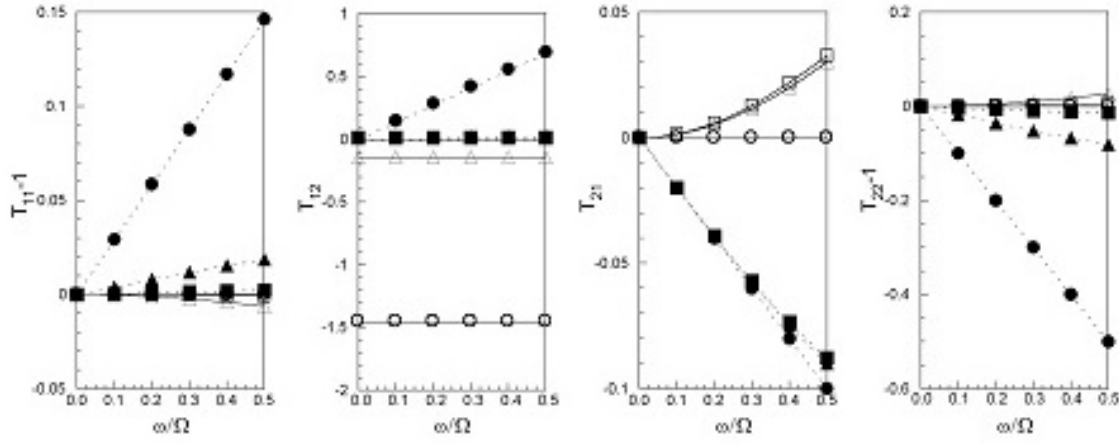
Figure 2: Calculated transfer matrices of the cavitating propeller for an advance ratio, $J_1 = 1.0$, and $(K^*/2\pi, M^*)=(0.1, 1.0)$ and for various values of $A^*/A_p = 1$ (○), 2 (△), and 10 (□), where open and closed symbols denote the real and imaginary parts of the matrix elements respectively.

propeller operated in a wider duct (for example $A^*/A_p = 10$) might be the most stable because of the large negative impedance with the small imaginary part of T_{22} and the large imaginary part of T_{21}.

Figure 3 presents the transfer matrix for an advance ratio of $J_1 = 1.0$, a duct cross-sectional area of $A^*/A_p = 2$ and various cavitation numbers. The values of $(K^*/2\pi, M^*)$ are again set to be $(0.1, 1.0)$ for all cases. Head deterioration due to the presence of cavitation is implicitly included through the assumed changes in the deviation angle β. All elements are affected by the head deterioration, but the stability does not seem to be significantly changed. The imaginary parts of both T_{21} and T_{22} are increased by the head deterioration.
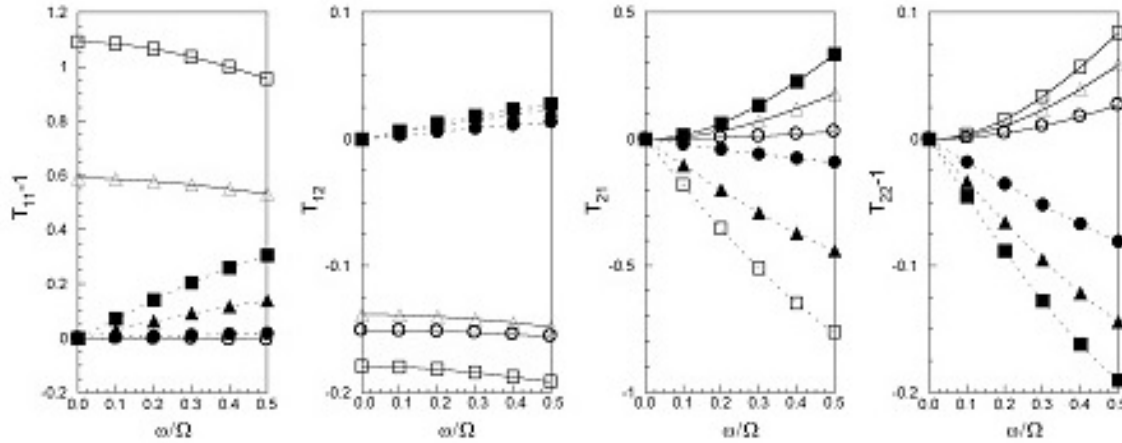

Figure 3: Calculated transfer matrices of the cavitating propeller for an advance ratio, $J_1 = 1.0$ and $A^*/A_p = 2$ for the various cavitation numbers $\sigma = \infty$ (○), 0.05 (△), and 0.01 (□), where open and closed symbols denote the real and imaginary parts of the matrix elements respectively.

To proceed we must develop values for the cavitation compliance and mass flow gain factor of a cavitating propeller. Otsuka *et al.* (1996) and Watanabe *et al.* (1998) have obtained the cavitation compliance and mass flow gain factor of cavitating cascades by a free streamline theory. Here, we utilize their results in order to estimate appropriate values of $K^*/2\pi$ and M^*. The values of $(K^*/2\pi, M^*)$ obtained by those

investigations are shown in Figure 4 for typical values for the solidity (1.0), the stagger angle ($\beta = 25°$) and the number of blades ($Z_R = 5$). Because Otsuka *et al.* (1996) and Watanabe *et al.* (1998) examine only two-dimensional flows around foils, the cavity size per blade is treated as a cross sectional area V_{cpb} (not a volume) and the scaling as $V_c = Z_R R V_{cpb}/2$ is used as a best estimate. Note that $(K^*/2\pi, M^*)$ are functions of the parameter $\lambda = \sigma^*/2\alpha$, where σ^* is the cavitation number *at inlet to the propeller*.
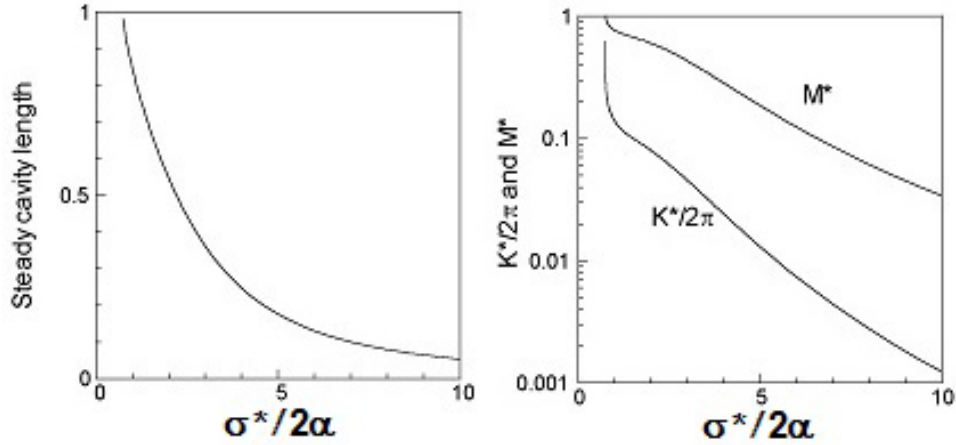

Figure 4: Steady cavity length and the quasi-static cavitation compliance and mass flow gain factor plotted against $\sigma^*/2\alpha$ obtained by a free streamline theory (Watanabe *et al.* 1998) for solidity $= 1.0$, stagger angle $\beta = 25°$ and $Z_R = 5$.

Now, rather than use the fixed values of K^* and M^*, we calculate the transfer function using the above relations between $(K^*/2\pi, M^*)$ and $\lambda = \sigma^*/2\alpha$. Results are shown in Figures 5 and 6 for $A^*/A_p = 2$ and 10, respectively. Three cases with different upstream cavitation numbers $\sigma = 0.15$, 0.20 and 0.5 are examined. The advance ratio J_1 is 1.0, which is larger than the critical value. Note that, only for the case with $\sigma = 0.15$, is the parameter $\lambda = \sigma/2\alpha$ less than unity and therefore only in this case is there head deterioration with increasing deviation angle. The cavitation compliance $K^*/2\pi$ varies from 0.018 to 0.172 for $A^*/A_p = 2$ and from 0.009 to 0.143 for $A^*/A_p = 10$. The mass flow gain factor M^* varies from 0.231 to 0.831 for $A^*/A_p = 2$ and from 0.140 to 0.777 for $A^*/A_p = 10$. These values are slightly smaller for the case with $A^*/A_p = 10$. This is because, as shown in Figure **??**, the flow coefficient is slightly larger for the case with $A^*/A_p = 10$, and this results in a smaller incidence angle.

From Figures 5 and 6, it is seen that T_{21} takes similar values for all the cavitation numbers, while the other elements of the transfer matrix are much affected by the presence of cavitation. Note that the elements $T_{11} - 1$, T_{12} and $T_{22} - 1$ are much smaller for the case with $A^*/A_p = 10$, whereas the element T_{21} is the same order for both cases. This implies that the propeller with $A^*/A_p = 10$ is more stable since the imaginary part of T_{22} is smaller; in other words the effective mass flow gain factor is smaller.

The advance ratio J_1 is also an important parameter, because there is a critical value which separates normal operation from pump-like operation. It would be interesting to compare the transfer matrices for normal and pump-like operations, but unfortunately the free streamline theory is only applicable for high flow rates and high advance ratios.

We now consider the dynamics of the whole system of the water tunnel, taking the experimental arrangement used by Duttweiler and Brennen (2002) as an example. Figure 7 shows the schematic of the facility and cavitation dynamics used by Duttweiler and Brennen. The facility dynamics are characterized by (i) the compliance, $C_{ot} = 405$, of the overflow tank that allows control of the pressure within the facility and therefore has the only deliberate free surface, (ii) the resistance, $R_c = 0.0295$, and inertance, $L_c = 57.3$, of
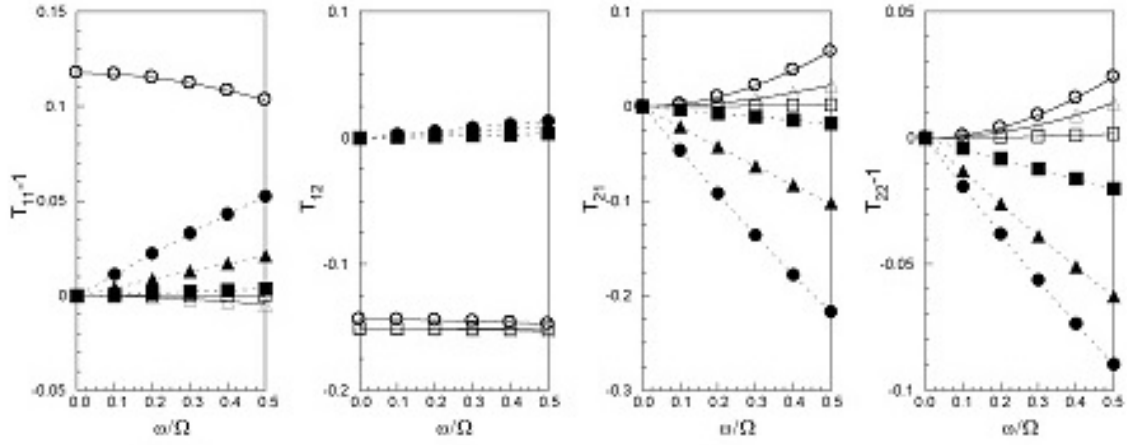
Figure 5: Calculated transfer matrices of the cavitating propeller with $A^*/A_p = 2$ and an advance ratio, $J_1 = 1.0$, for the various cavitation numbers $\sigma = 0.15$ (○), 0.20 (△), and 0.50 (□) where open and closed symbols denote real and imaginary parts of matrix elements respectively. The values of cavitation compliance and mass flow gain factor are obtained from Figure 4.
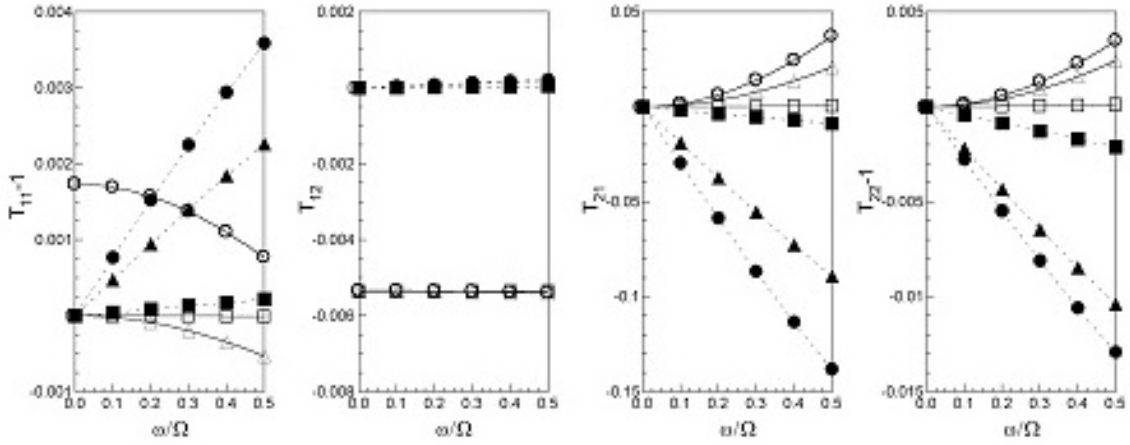

Figure 6: Calculated transfer matrices of the cavitating propeller with $A^*/A_p = 10$ and an advance ratio, $J_1 = 1.0$, for the various cavitation numbers $\sigma = 0.15$ (○), 0.20 (△), and 0.50 (□) where open and closed symbols denote real and imaginary parts of matrix elements respectively. The values of cavitation compliance and mass flow gain factor are obtained from Figure 4.

the pipe connecting the tunnel with the overflow tank, (iii) the compliance, $C_t = 1970$, associated with the expansion and contraction of the walls of the tunnel, and (iv) the resistances, $R_{tu} = 0.0$ and $R_{td} = 0.0$, and inertances, $L_{tu} = 0.953$ and $L_{td} = 2.10$, associated with the typical flow paths upstream and downstream of the cavitating propeller. The parameters used by Duttweiler and Brennen (2002) were normalized using the propeller radius, R, and the propeller rotation frequency, Ω, to obtain the values shown in the square brackets after each symbol.

The dynamics of the system can be characterized by considering the response of the system to a fluctuating mass flow rate, $\tilde{m}_e$, injected at some specific location, e, in the system (Figure 7). We define a system impedance, Z, as $Z = \tilde{p}_e^T/\tilde{m}_e$ where $\tilde{p}_e^T$ is the total pressure fluctuation at e. Note that, in general, the impedance Z is complex.

Using the present methodology coupled with the dynamics of the water tunnel identified by Duttweiler and Brennen (2002), we have calculated the system impedance Z for the case with advance ratio $J_1 = 0.64$ and
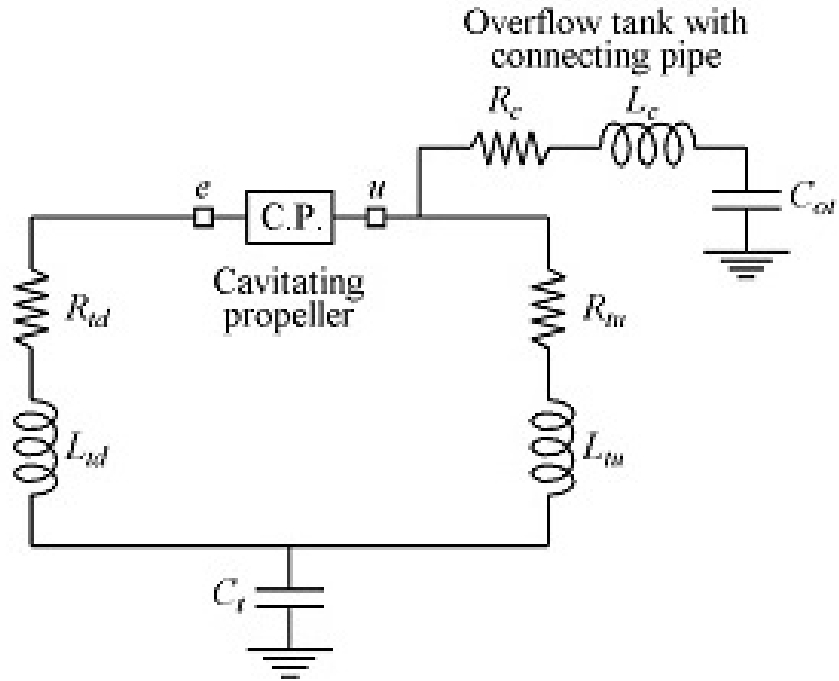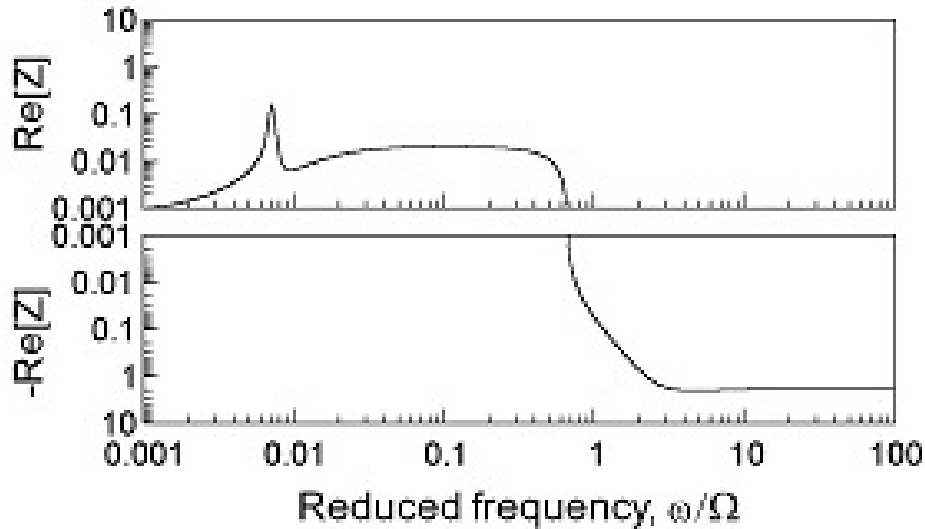
Figure 7: Schematic of facility and cavitation dynamics.

Figure 8: An example of the system impedance, Z. The mass flow fluctuation is imposed at the point e in Figure 7. The real part of the system impedance is plotted against the various excitation frequencies For $J_1 = 0.64$, $\sigma = 0.25$ and with K^* and M^* evaluated from Figure 4.

cavitation number $\sigma = 0.25$. The real part of Z is plotted in Figure 8 against the normalized frequency, ω/Ω. In calculating the transfer matrix of propeller, we set $A^*/A_p = 3.16$ and $Z_R = 6$ and the cavitation characteristics (M, K) shown in Figure 4 were used. The positive peak at $\omega/\Omega = 0.007$ is largely due to the impedance of overflow tank. The shallow negative peak around $\omega/\Omega = 3$ might indicate the existence of surge instability, but the frequency is much higher than the value of $\omega/\Omega = 0.2$ observed in the experiments of Duttweiler and Brennen (2002). Moreover, if we compare the present result with the system impedance obtained by Duttweiler and Brennen, we find that the frequency obtained by the present analysis is still

much higher than the experimental values and the peak is much shallower. The explanation for this discrepancy is unknown, but the following may be pertinent. In the pump cases, the elements T_{21} and $T_{22} - 1$ are purely imaginary when the cavitation compliance and mass flow gain factor considered are purely real. On the other hand, in the propeller cases, T_{21} and $T_{22} - 1$ are complex because of our one-dimensional flow tube model. Complex values of T_{21} and $T_{22} - 1$ mean that the system responds as if the cavitation compliance and mass flow gain factor were complex.
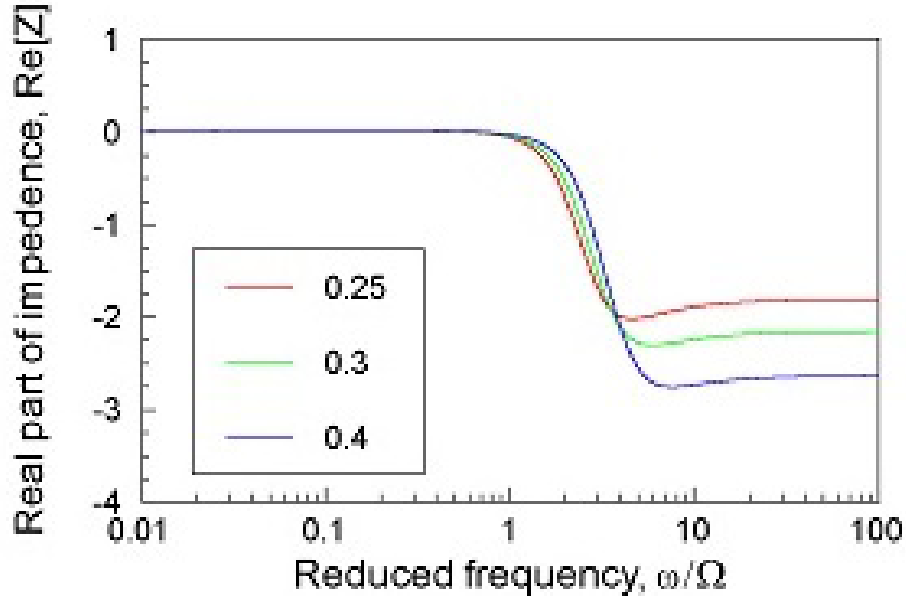

Figure 9: The real part of the system impedance for various upstream cavitation numbers, σ as indicated, for $J_1 = 0.64$ and for K^* and M^* evaluated from Figure 4.

Figure 9 shows the real part of system impedance for the case with three different cavitation numbers, $\sigma = 0.25$, 0.2 and 0.15. The frequency at the negative peak decreases as the cavitation number is decreased, but is still larger than the experimental value of $\omega/\Omega = 0.2$. One possible explanation for the discrepancy is that the model considers only the sheet cavitation on the blade surface. However, a large volume change in the tip cavity during a surge cycle was clearly observed in experiments by Duttweiler and Brennen (2002). It is important to note that the present one-dimensional stream tube model may lose validity at the lower advance ratios, at which the flow around the propeller is very three-dimensional. However, because the surge instability is a system instability in which a large amount of fluid is accelerated one-dimensionally by the volume change of the cavitation, the present method is expected to be applicable even at those low advance ratios provided we could evaluate the cavitation compliance and the mass flow gain factor for all the cavitation including the tip vortex cavities. The unsteady characteristics of tip vortex cavities need further investigation.

Figure 10 shows the values of $\sigma^*/2\alpha$ just upstream of the propeller plotted in a graph of σ against J_1 obtained by the present steady analysis. According to the linear theory [11], cavitation instabilities of a 2-D cascade are dependent only on the parameter $\sigma/2\alpha$. The instability boundary obtained by Duttweiler and Brennen (2002) is also plotted in the figure. We can see that the value of $\sigma^*/2\alpha$ is nearly constant along the instability boundary, which means that the stability depends on the local condition at the propeller inlet rather than the advance ratio or upstream cavitation number.

Thus we have evaluated the quasi-static transfer matrices for a cavitating propeller operating in a water tunnel. Simple flow models based on a one-dimensional flow tube analysis are used. The effects of
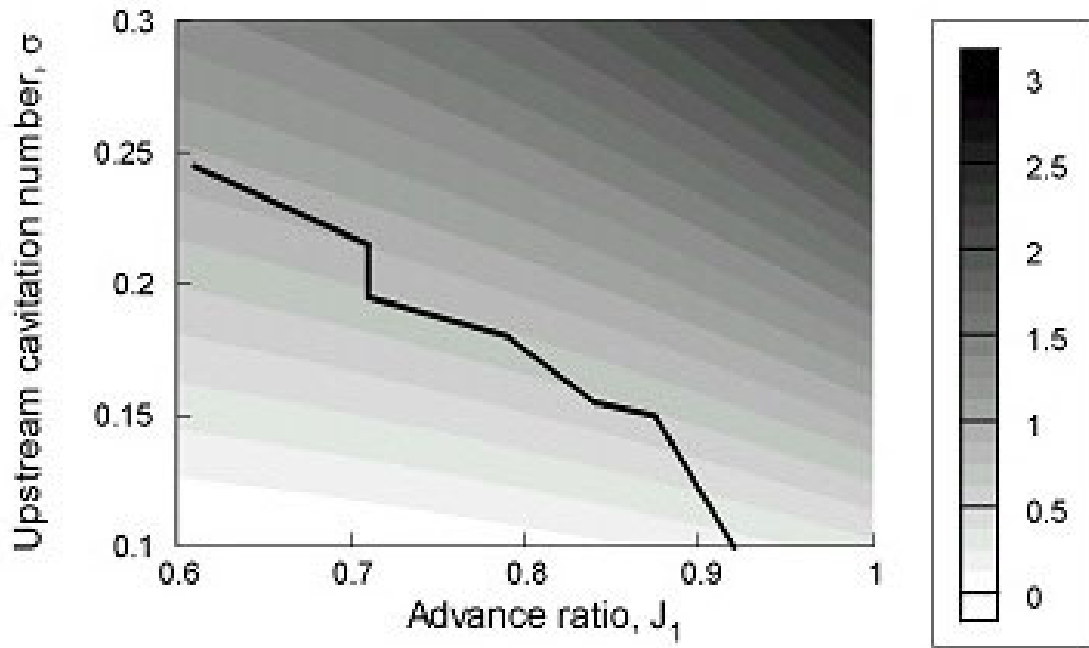
Figure 10: The ratio of cavitation number to incidence angle (divided by 2), $\sigma^*/2\alpha$, plotted against the advance ratio J_1 for various upstream cavitation numbers, σ. The solid line is the boundary of the onset of surge instability observed by Duttweiler and Brennen (2002). Surge instability occurs in the region below this line.

the presence of cavitation, and of the blockage due to the tunnel walls are examined. The former is modeled by the head deterioration through the deviation of the exit flow, and the conventional cavitation characteristics, the cavitation compliance and the mass flow gain factor. These characteristics are estimated by a free streamline theory. It is found that the presence of the tunnel wall has a large effect on the stability of propeller operation. In an open condition, the flow rate through the propeller is not very sensitive to the advance ratio. However, in the presence of the tunnel walls, the propeller flow rate changes much more in response to the advance ratio change. This implies that, if there are flow rate fluctuations, the flow rate through the propeller varies more when there are tunnel walls and this may result in unstable operation of the propeller. When the advance ratio is the same, the flow rate through the propeller is smaller and the incidence angle is larger if the propeller is operated in a tunnel with a smaller cross-sectional area. Large incidence angles can result in the flow instabilities and enhance the occurrence of cavitation. Transfer matrices for the cavitating propeller are evaluated by assuming the flow is quasi-static. The transfer matrices show that the propeller operating in the narrower tunnel is much more unstable. If the propeller is operated in a wider tunnel or in an open condition, the effects of a mass flow gain factor are reduced because the variation of the propeller flow rate is smaller even when the total flow rate changes substantially.